Two-phase, Steam-water Critical Flow

H. S. ISBIN, J. E. MOY, and A. J. R. DA CRUZ

University of Minnesota, Minneapolis, Minnesota

Two-phase critical flow of steam-water mixtures has been investigated over a pressure range from 4 to 43 lb./sq. in. abs. and a quality range from saturated vapor to 1% (weight) vapor. Discharges were measured from 1/4-, 1/2-, 3/4-, and 1-in. pipes and from annuli of intermediate cross-sectional areas. The experimental mass flow rates are always greater than the values calculated on the basis of a homogeneous flow model. Several empirical methods for correlating the data were determined, and comparisons are presented of the predictions of several analytical flow models.

Critical flow occurs when the velocity of the fluid is equal to that of the propagation of the pressure wave. Single-phase critical flow can be predicted, but thus far no reliable theory has been established for two-phase. This study is concerned with the concurrent flow of steam-water mixtures.

The flow of flashing-water mixtures has received considerable attention (*1* to *5, 8, 10, 12, 17, 18, 19*) and the existence of two-phase–critical-flow behavior has been noted (*1, 3, 4, 5, 7, 12, 15, 16, 18*), but with the exception of the flow tests undertaken by C. Robbins* this investigation represents the first study undertaken explicitly to measure critical flows of steam-water mixtures over a wide range of quality. Critical flow of vapor-liquid mixtures occurs in many engineering and industrial applications, such as the handling of condensed gases and refrigerants, drains, and blow-offs from boilers and turbines, and in coolant designs for nuclear reactors.

EXPERIMENTAL

Figure 1 is a schematic sketch of the flow equipment used to investigate the critical flow behavior of steam-water mixtures. Steam and water flows were mixed, passed through a horizontal test section, and then discharged into an enlarged pipe which was connected directly to a condenser. The total mass flow to the test section was readily set and controlled—independent of the pressure regulation in the condenser—by throttling separately the supply of steam and water to the mixer. Changes in the downstream pressure (in the expansion section) served to change only the axial pressure distribution in the test section and not the discharge rates. The pressure drops along the length of the test section were measured to about 1 diam. of the discharge end. Figure 2 illustrates the pressure profiles for the test section for changes in downstream pressure. Nearly all runs were made with a downstream pressure of 1 lb./sq. in. abs., and the critical pressure in the test section at the discharge was determined by extrapolating the pressure profiles to the end of the pipe; however, it is to be noted that even at this low downstream pressure the effects on the pressure profile did not entirely disappear. The propagation of pressure disturbances through a thin liquid annulus is not unexpected.

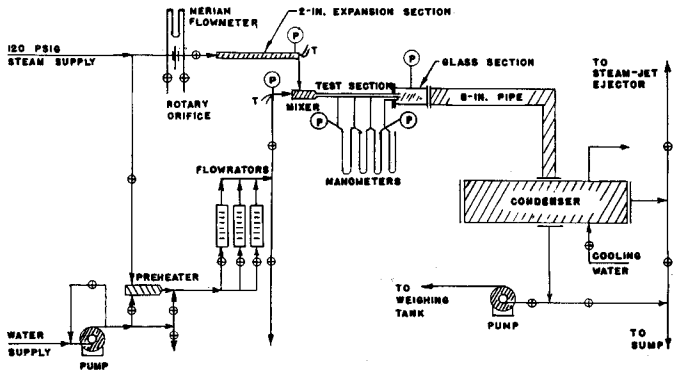

Fig. 1. Schematic sketch of critical steam-water flow equipment.

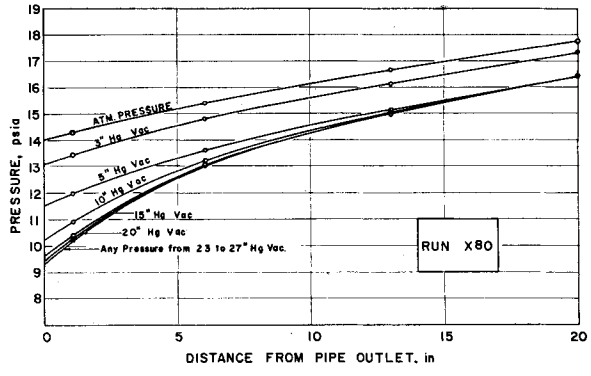

Fig. 2. Variation in pressure profile as downstream pressure varies between atmospheric and 27 in. Hg.

J. E. Moy is now with the Glenn L. Martin Company, Baltimore, Maryland, and A. J. R. da Cruz is completing U. S. Army service.

*Classified studies at the General Electric Company, Richland, Washington.

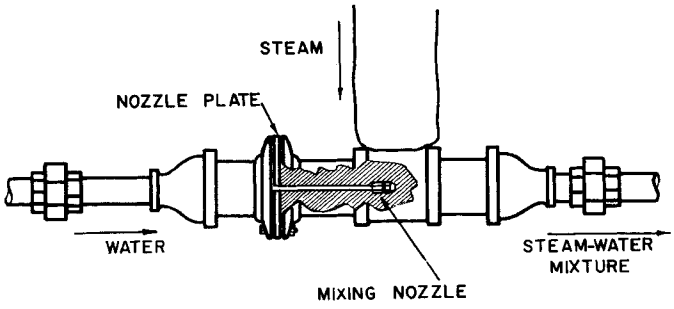

Fig. 3. Diagram of steam-water mixer showing installation of nozzle.

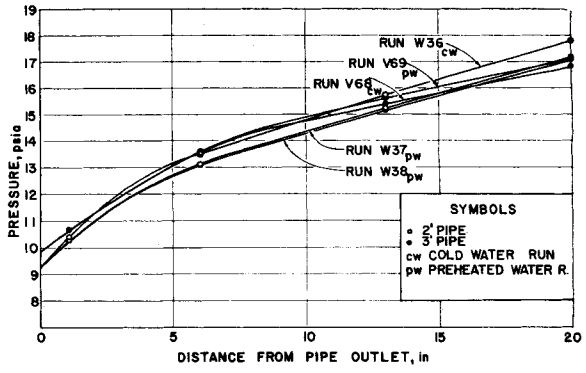

Fig. 4. Comparison of cold-water runs with preheated-water runs.

Considerable attention was directed to the method of mixing the steam and water flows. The diagram of the steam-water mixer is given in Figure 3. Mixing conditions included a variety of spray nozzles, 2- and 3-ft. test sections, and cold and preheated water with proportionately different steam flows to provide the same desired exit quality. Typical comparisons of the effects of pipe length and water preheat are shown in Figure 4. The effect of mixing on the evaluation of the critical discharge pressure was found to be within the experimental error of extrapolating the pressure profile curves (about 0.1 lb./sq. in. abs. in the 5 to 20 lb./sq. in abs. range, and about 0.5 lb./sq. in. abs. in the 25 to 45 lb./sq. in. abs. range). The method of mixing affected the pressure profiles, but the 2-ft. test section was sufficiently long so that the values determined for the critical pressure were independent of the method of mixing.

The total energy of the discharge stream was determined by measuring separately the flow rates and enthalpies of the steam and water feeds to the mixer. Calculated kinetic-energy terms were included when significant.

Four full-bore test sections were used consisting of stainless steel pipes ¼, ½, ¾, and 1 in. in diam.; and two annuli were formed by placing a ¼-in. brass pipe inside the ¾- and 1-in. pipes and supporting it by three brass pins. The discharge of each test section had a sharp, flat cross section. Data for the test sections are summarized in Table 1. Critical flow occurred within the test section at the discharge end. The experimental critical two-phase flow conditions were defined by the total measured flow rate of water and steam to the test section, calculated total energy of the flowing stream in the test section, and the extrapolated pressure in the test section at the discharge for a downstream pressure of 1 lb./sq. in. abs

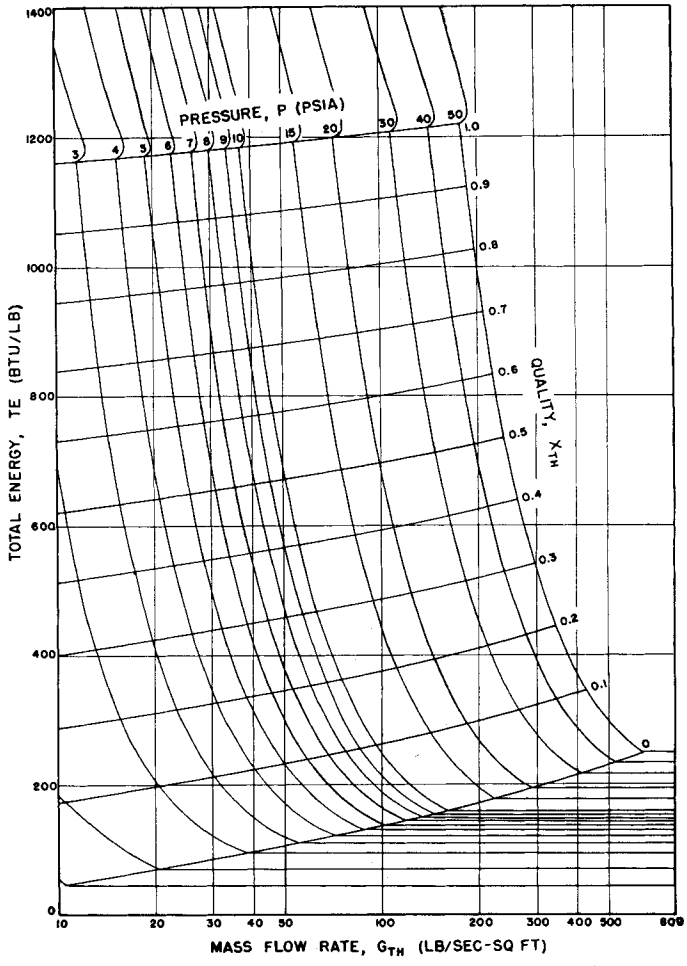

Fig. 5. Theoretical critical discharges for steam-water mixtures (homogeneous model).

Table 1. Test Sections

Nominal pipe size, full-bore	Inside diameter, in.	Cross-sectional area, sq. ft.	I.D.,† in.	Pressure taps Distance from discharge end, in. Tap number 1	2	3	4
1/4	0.3743	0.0007641	1/16	1/2	5	11	18-1/2
1/2	0.6249	0.002130	1/16	1/2	5	11	18-1/2
3/4	0.8188	0.003657	3/32	3/4	5-1/2	11-1/4	18-3/4
1	1.0425	0.005927	1/8	1-3/32	6-1/32	13	20
Annulus 3/4–1/4*		0.002068		Same as 3/4-in. full bore			
1–1/4		0.004324		Same as 1-in. full bore			

*¼ brass pipe, 0.5398 in. O.D. The distances of the supporting pins from the pipe outlet were 9.937 and 8.550 in. for the 1—¼ = and ¾—¼ annuli, respectively. (The inlet ends were separately supported.)
†I. D. of pressure tap.

EXPERIMENTAL DATA

The extensive data of Cruz for the 1-in.–diam. test section are tabulated in reference *6*, and the data of Moy (*14*) are summarized in Table 2. Values tabulated are as follows: G, critical mass flow rate (total flow rate); P, critical pressure; TE, total specific energy of the two-phase flow; and x_{th}, a calculated value which

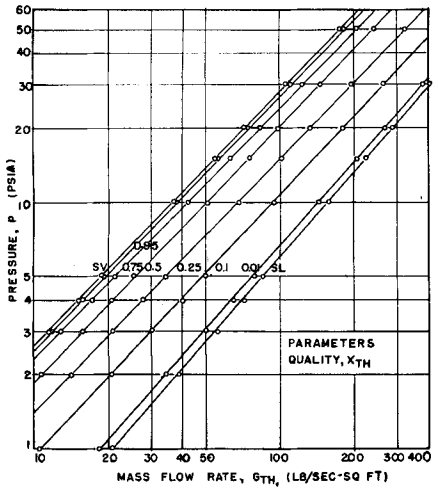

Fig. 6. Theoretical critical mass flow rates of steam-water mixtures as a function of critical pressure (homogeneous model).

represents the quality of the two-phase flow for the given conditions of P and TE, on the assumption that the flow is a homogeneous mixture at a uniform velocity and with the liquid and vapor at equilibrium. The evaluation of a true quality at the discharge end of the test requires detailed information on the kinetic energies of each of the phases.

CORRELATION OF DATA

Homogeneous Model

The application of single-phase theory to the homogeneous model requires the following assumptions: (1) the flow mixture is homogeneous and is flowing at a uniform velocity with the phases in equilibrium and (2) the critical-flow condition is defined under the restraints that the change in mass flow rate with respect to the pressure is zero at constant entropy. Under these conditions the critical mass flow rate is defined by the relation

$$G^2 = -g_c\left(\frac{dp}{dv}\right)_s \qquad (1)$$

where v is the mixture specific volume and is equal to $v_f + xv_{fg}$. Values for G calculated with Equation (1) are referred to as theoretical values, or G_{th}. Figure 5 illustrates the relations between total specific energy TE, critical mass flow rate G, critical pressure P, and quality x for steam-water flows based upon the homogeneous model. The quality is calculated through the use of the total energy relation:

$$TE = h_f + xh_{fg} + [(v_f + xv_{fg})]G^2/2g_cJ \qquad (2)$$

The logarithmic plot of G vs. P yields nearly parallel straight lines with the quality as a parameter (see Figure 6), and the logarithmic plot of $G/P^{0.96}$ vs. x (Figure 7) serves to bring the curves together over the range of quality from 1 to 0.1. The points indicated on Figures 6 and 7 are calculated values.

Empirical Correlations

Cruz noted that the plot of $[(G_{OB} - G_{TH})/G_{OB}]$ 100, percentage of deviation, vs. quality, x_{th}, served to correlate his data for the 1-in.-diam. test section, independent of the critical pressures. The subscript OB refers to the experimental (observed) data, and TH refers to the homogeneous-flow-model calculations (theoretical). Moy's data, to-

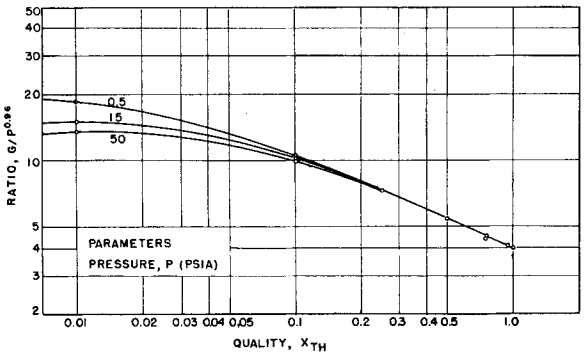

Fig. 7. Empirical representation of theoretical critical mass flow rates of steam-water mixtures (homogeneous model).

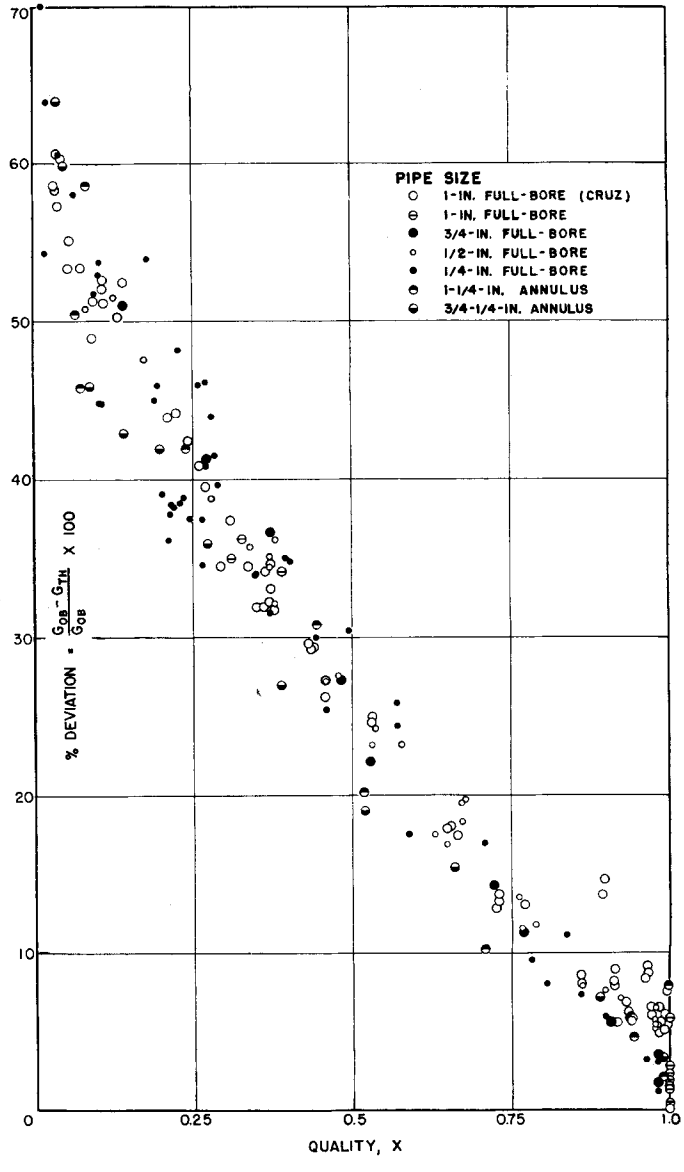

Fig. 8. Empirical correlation of experimental data on critical steam-water mass-flow-rate deviations from theoretical values.

TABLE 2. TWO-PHASE, STEAM-WATER, CRITICAL-FLOW DATA
(Downstream pressure at 1 lb./sq. in. abs.)

Run	G	TE	P	x_{th}	Run	G	TE	P	x_{th}
				1-in. full bore					
91	26.2	1175.6	6.9	0.999	96	34.5	1180.9	8.75	1.000
92	32.4	1177.7	8.5	0.996	97	22.4	1170.1	5.75	0.998
93	20.8	1177.1	5.4	1.000	98	80.5	557.2	9.4	0.390
94	22.5	1177.7	5.8	1.000	99	92.6	492.6	9.5	0.327
95	22.8	1179.4	7.4	1.000	100	92.4	473.8	9.4	0.310
				3/4-in. full bore					
194	66.1	1180.4	18.2	0.985	199	96.3	666.0	13.7	0.484
195	66.3	1180.3	17.8	0.985	200	78.9	532.9	8.5	0.372
196	110.5	722.3	17.8	0.530	201	46.7	899.6	9.3	0.725
197	82.3	962.5	18.1	0.770	202	100.6	432.1	8.9	0.272
198	71.0	1099.2	17.7	0.908	203	148.8	294.8	8.5	0.140
				1/2-in. full bore					
160	79.5	536.6	9.0	0.372	177	98.0	660.9	13.8	0.479
161	80.1	536.0	8.9	0.373	178	81.0	546.4	9.5	0.378
162	73.4	857.3	13.5	0.675	179	51.7	823.3	9.5	0.650
163	66.6	1178.5	17.5	0.985	180	104.6	445.7	9.7	0.280
165	56.0	750.1	9.0	0.580	181	168.9	283.4	9.2	0.125
166	79.8	543.5	8.8	0.380	182	168.9	283.5	9.2	0.125
167	73.9	861.3	13.4	0.675	183	348.9	269.8	17.6	0.081
168	79.9	541.4	8.8	0.380	184	257.8	360.5	17.6	0.173
169	74.7	865.1	13.6	0.680	185	160.3	529.3	17.6	0.340
170	67.6	1176.5	17.7	0.980	186	126.4	648.9	17.7	0.460
171	112.1	726.3	17.7	0.538	187	95.8	845.4	17.8	0.630
172	83.7	960.7	17.8	0.770	188	80.5	969.9	17.6	0.790
173	67.5	1175.9	17.8	0.980	189	73.8	1058.1	17.7	0.865
174	112.0	726.0	17.8	0.533	190	71.0	1120.1	17.8	0.924
175	83.3	958.7	17.8	0.766	191	68.4	1174.0	17.7	0.980
176	72.5	1090.7	17.6	0.900					
				1/4-in. full bore					
230	90.0	1180.8	23.8	0.980	239	565.5	231.2	19.2	0.039
231	102.2	1039.0	23.2	0.838	240	638.3	211.5	18.1	0.022
232	114.4	912.3	22.4	0.710	241	691.3	192.2	15.0	0.010
233	133.5	769.9	21.6	0.573	242	895.0	238.8	33.2	0.017
234	173.4	599.5	20.6	0.405	243	562.8	333.1	36.0	0.107
235	213.5	485.4	20.4	0.290	244	370.1	435.6	34.5	0.212
236	275.6	389.2	20.3	0.195	245	343.9	483.5	34.0	0.265
237	401.0	293.6	20.9	0.095	246	292.6	596.3	36.8	0.372
238	477.5	264.5	21.3	0.063	247	249.3	681.4	37.0	0.460
248	213.5	811.7	39.7	0.590	284	62.2	411.0	5.0	0.270
249	179.0	1001.7	40.8	0.783	285	35.0	1165.0	9.0	0.985
250	173.9	1025.5	40.8	0.808	286	68.9	511.0	7.6	0.350
251	168.3	1079.0	41.1	0.862	287	46.5	735.0	7.2	0.572
252	165.7	1116.4	41.9	0.900	288	38.4	644.0	5.2	0.495
253	159.9	1180.0	43.0	0.965	289	51.0	496.0	5.07	0.350
275	362.8	421.5	31.7	0.202	290	79.1	312.0	4.5	0.180
276	316.7	428.6	28.5	0.215	292	46.2	509.0	4.4	0.370
277	290.7	420.6	25.6	0.215	293	206.0	265.0	10.2	0.102
278	254.7	420.2	22.7	0.220	294	206.0	264.0	10.0	0.102
279	217.9	423.0	19.6	0.230	295	111.2	341.0	7.9	0.190
280	179.7	421.0	16.0	0.235	296	90.0	430.0	8.0	0.272
281	144.1	422.3	13.2	0.245	297	80.5	412.5	6.4	0.260
282	109.4	433.6	10.7	0.264	298	60.8	423.0	5.15	0.280
283	73.6	439.0	6.6	0.285	299	56.5	354.0	3.9	0.227
				1-1/4 in. annulus					
209	184.6	233.8	9.6	0.075	214	73.4	1140.0	18.9	0.945
210	59.4	1181.1	16.0	0.991	215	76.6	616.0	9.9	0.445
211	191.5	428.0	16.9	0.240	216	35.3	1186.2	8.8	1.000
212	115.2	711.0	18.6	0.518	217	185.8	238.8	8.3	0.085
213	89.1	904.0	18.9	0.710	218	185.9	218.8	8.3	0.067
				3/4–1/4 in. annulus					
219	58.9	1184.1	15.7	0.993	225	189.5	382.8	15.1	0.200
220	64.6	1083.0	15.6	0.893	226	221.0	328.8	15.1	0.145
221	82.7	851.8	16.0	0.663	227	285.5	261.0	15.3	0.080
222	96.3	703.9	15.9	0.520	228	350.2	220.8	12.5	0.050
223	119.1	570.7	15.5	0.390	229	390.4	201.3	11.5	0.036
224	156.4	459.9	15.4	0.275					

gether with those of Cruz, are given in Fig. 8. The empirical relation noted for the homogeneous flow model, Figure 7, was used to plot the experimental critical mass flow rate and critical pressure data as a function of the calculated quality, x_{th}. Figure 9 illustrates the effectiveness of this empirical correlation.

Analytical Models

One simple approach to the critical two-phase flow is to assume an annular flow with a central gas core with the sonic velocity of the gas core limiting the total flow. If the void fraction data of Martinelli (*13, 9*) or the estimated values of Levy (*11*) are used, it is found that this approach leads to values for the critical flow which are well above the experimental measurements. For example, the value of R_g would have to be about 0.3 to conform to the observed discharges for qualities as low as 0.050; whereas the Martinelli and Levy R_g values are 0.9 and 0.7.

A more detailed approach is based upon a momentum balance initially derived by Linning (*12, 9*), which incorporates several simplifying assumptions. In an annular flow model with gas flowing at a uniform velocity in the core and the liquid flowing at a uniform velocity in an annulus at the wall, the pressure at a cross section is considered to be uniform. For the conditions of steady and isentropic flow (to evaluate maximum flow).

$$d(W_g u_g + W_f u_f) = -A\,dp \qquad (3)$$

The phase velocities are expressed in terms of the void fractions, quality, and the total mass flow rate:

$$u_g = \frac{xGv_g}{R_g} \qquad (4)$$

$$u_f = \frac{(1-x)Gv_f}{(1-R_g)} \qquad (5)$$

Further, $W_g = xGA$ and $W_f = (1-x)GA$. With these substitutions and the differentiation carried out under constant entropy, Equation (3) becomes

$$-1 = \frac{G^2}{g_c}\left[\left\{\frac{2xv_g}{R_g} - \frac{2(1-x)v_f}{1-R_g}\right\}\left(\frac{dx}{dp}\right)_s + \left\{\frac{(1-x)^2}{1-R_g}\right\}\left(\frac{dv_f}{dp}\right)_s + \frac{x^2}{R_g}\left(\frac{dv_g}{dp}\right)_s + \left\{\frac{(1-x)^2 v_f}{(1-R_g)^2} - \frac{x^2 v_g}{R_g^2}\right\}\left(\frac{dR_g}{dp}\right)_s\right] \qquad (6)$$

Martinelli's correlation of R_g may be represented by a straight line over limited ranges:

$$R_g = aX + b \qquad (7)$$

where a and b are constants to be determined for each range and

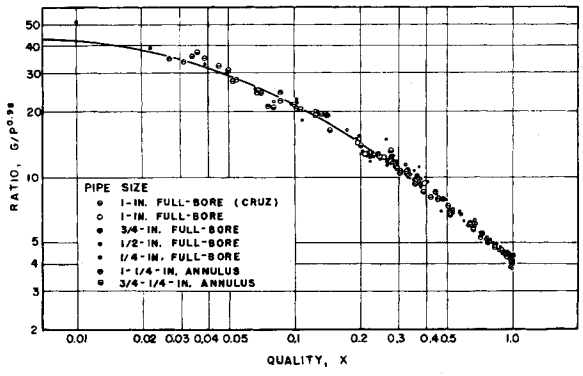

Fig. 9. Empirical correlation of experimental data on critical steam-water mass flow rates.

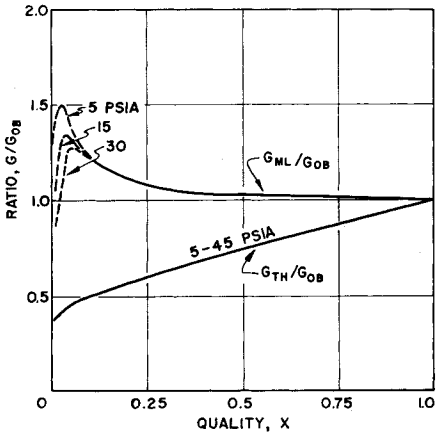

Fig. 10. Comparison of calculated mass flow rates with observed values.

$$X^2 = \left(\frac{1-x}{x}\right)^{1.8}\left(\frac{v_f}{v_g}\right)\left(\frac{\mu_f}{\mu_g}\right)^{0.2}$$

$$= f(x, p) \text{ for steam-water} \qquad (8)$$

An approximation of the term $(dR_g/dp)_s$ is then

$$\frac{1}{a}\left(\frac{dR_g}{dp}\right)_s = \left(\frac{dX}{dx}\right)_p\left(\frac{dx}{dp}\right)_s + \left(\frac{dX}{dp}\right)_x \qquad (9)$$

Thus with the use of the steam tables and the empirical evaluations from the Martinelli correlation, Equation (6) can be solved for G for given values of x and p. The use of the modified momentum model leads to results shown in Figure 10. Agreement is good at the higher qualities and the predicted values become increasing larger than the observed values as the quality is decreased. At 10% quality the ratio of the predicted to the observed value is as high as 1.24. The ratio G_{TH}/G_{OB} is included in Figure 10 for comparison of the modified momentum model and the homogeneous model.

COMPARISON WITH OTHER INVESTIGATORS

Benjamin and Miller's data on flashing water for 4-in. pipes (*3*) are closely approximated by the homogeneous model and thus are not in agreement with the empirical correlations given in Figures 8 and 9. Similarly, the Bottomley mass flow data (*4*) for 3 to 4% quality at critical pressures from 35 to 53 lb./sq. in. abs. are significantly lower than the observed values in this paper.

Burnell's data (*5*) for boiling-water discharge from ½- to 1½-in. pipes agreed within ±10% with the discharges calculated from the empirical correlations for a pressure range from 6 to 15 lb./sq. in. abs. and were 20 to 35% lower for a pressure range from 25.4 to 58.5 lb./sq. in. abs. The Burnell nozzle-discharge data ranged from 3.4 to 34.1% less than the empirical values based upon the correlations.

Comparisons were made with Linning's predicted discharge values (*12*) for qualities from 1 to 10%. The Linning values were about 40 to 50% less than the observed values in this paper.

SUMMARY

A new method of measuring the critical flow behavior of steam-water mixtures has been described. In general, the critical flows measured are higher than the results reported previously by investigators studying the flow of flashing water. The inadequacy of the homogeneous model for evaluating critical discharges for low qualities has been demonstrated. Two empirical correlations were developed, but these correlations should be limited to the range of variables studied. Several analytical approaches were tried and a modified momentum model yielded the best results over a quality range from 1 to 0.1. Considerable progress has yet to be made in defining and understanding the two-phase critical-flow phenomena.

ACKNOWLEDGMENT

The investigations reported were made possible through an Atomic Energy Commission contract AT-(11-1)-210, 211 with the Chemical Engineering Department, University of Minnesota.

NOTATION

A = flow cross-sectional area, sq. ft.
a, b = empirical constants
G = mass flow rate, lb./(sec.)(sq. ft.)
g_c = gravitational constant, 32.2 lb.$_m$-ft./lb.$_f$-sec.^{2}
h = enthalpy, B.t.u./lb.
J = conversion factor, 778 ft.-lb./B.t.u.
P = critical pressure, lb./sq. in. abs.
R_g = void fraction, fraction of cross-sectional area occupied by the gas
s = entropy, B.t.u./(lb.)(°F.)
TE = total specific energy, B.t.u./lb.
u = velocity, ft./sec.
v = specific volume, cu. ft./lb.
W = mass rate, lb./sec.
x = quality
μ = viscosity, lb.$_m$/(ft.)(sec.)

Subscripts

f = saturated liquid phase
fg = change by evaporation
g = gas phase
OB = observed or experimental
TH or th = theoretical (calculated on basis-of homogeneous model)

LITERATURE CITED

1. Allen, W. P. Jr., *Trans. Am. Soc. Mech. Engrs.*, **73**, 257 (1951).
2. Bailey, J. F., *ibid.*, 1109 (1951).
3. Benjamin, M. W., and J. G. Miller, *Trans. Am. Soc. Mech. Engrs.*, **64**, 657 (1942).
4. Bottomley, W. T., *Trans. Northeast Coast Institution of Engineers and Shipbuilders*, **53**, 65 (1936–7).
5. Burnell, J. G., *Engineering*, **164**, 572 (1946).
6. Cruz, A. J. R., M.S. thesis, Univ. of Minnesota, Minneapolis (1953).
7. Harvey, B. F., and A. S. Foust, *Chem. Eng. Progr. Symposium Ser.* No. **5**, **49**, 91 (1953).
8. Hodkenson, B., *Engineering*, **143**, 629 (1937).
9. Isbin, H. S., R. Moen, and D. R. Mosher, *AECU*-2994 (1954).
10. Kittredge, A. E., and E. S. Dougherty, *Combustion*, **6**, 14 (1934).
11. Levy, S., *Proc. Second Midwestern Conference on Fluid Mechanics*, p. 237, Ohio State University, Columbus (1952).
12. Linning, D. L., *Proc. Inst. Mech. Engrs.* (*B*), **1**, 64 (1952).
13. Martinelli, R. O., and R. W. Lockhart, *Chem. Eng. Progr.*, **45**, No. 1, 39 (1949).
14. Moy, J. E., M.S. thesis, Univ. of Minnesota, Minneapolis (1955).
15. Rateau, A., "Experimental Researches on the Flow of Steam Through Nozzles and Orifices and the Flow of Hot Water," trans. by H. B. Brydon, Constable, London (1905).
16. Schweppe, J. L., and A. S. Foust, *Chem. Eng. Progr. Symposium Ser.* No. **5**, **49**, 77 (1953).
17. Silver, R. S., *Proc. Roy. Soc.* (*London*) **A194**, 464 (1948).
18. Silver, R. S., and J. A. Mitchell, *Trans. Northeast Coast Institution of Engineers and Shipbuilders*, **62**, 51, D15-30 (1945–6).
19. Stuart, M. D., and D. R. Yarnall, *Mech. Eng.*, **58**, 481 (1936); *Trans. Am. Soc. Mech. Engrs.* **66**, 387 (1944).